Draft version February 1, 2008
Preprint typeset using LaTeX style emulateapj v. 10/09/06

UNVEILING OBSCURED ACCRETION IN THE CHANDRA DEEP FIELD SOUTH

F. Fiore[1], A. Grazian[1], P. Santini[1,2], S. Puccetti[3], M. Brusa[4], C. Feruglio[1], A. Fontana[1], E. Giallongo[1], A. Comastri[5], C. Gruppioni[5], F. Pozzi[6], G. Zamorani[5], C. Vignali[6]

Draft version February 1, 2008

ABSTRACT

We make use of deep HST, VLT, Spitzer and Chandra data on the Chandra Deep Field South to constrain the number of Compton thick AGN in this field. We show that sources with high 24μm to optical flux ratios and red colors form a distinct source population, and that their infrared luminosity is dominated by AGN emission. Analysis of the X-ray properties of these extreme sources shows that most of them (80$\pm$15%) are indeed likely to be highly obscured, Compton thick AGNs. The number of infrared selected, Compton thick AGNs with 5.8μm luminosity higher than $10^{44.2}$ erg s^{-1} turns out to be similar to that of X-ray selected, unobscured and moderately obscured AGNs with 2-10 keV luminosity higher than 10^{43} erg s^{-1} in the redshift bin 1.2-2.6. This "factor of 2" source population is exactly what it is needed to solve the discrepancies between model predictions and X-ray AGN selection.

Subject headings: Active Galactic Nuclei

1. INTRODUCTION

Active Galactic Nuclei (AGN) are not only witnesses of the phases of galaxy formation and/or assembly, but are most likely among leading actors. Indeed, three seminal discoveries indicate tight links and feedbacks between super-massive black holes (SMBH), nuclear activity and galaxy evolution. The first is the discovery of SMBH in the center of most nearby bulge dominated galaxies, and the tight correlation between their masses and galaxy bulge properties (Gebhardt et al. 2000, Ferrarese & Merritt 2000, Marconi & Hunt 2003 and references therein). The second is that the growth of SMBH is mostly due to accretion of matter during their active phases, and therefore that most bulge galaxies passed a phase of strong nuclear activity (Soltan 1982, Marconi et al. 2004). The third is that the evolution of AGN is luminosity dependent, with lower luminosity AGN peaking at a redshift lower than luminous QSOs (Hasinger 2003, 2005, Fiore et al. 2003, Ueda et al. 2003, La Franca et al. 2005, Brandt & Hasinger 2005, Bongiorno et al. 2007), a bimodal behavior recalling the evolution of star-forming galaxies and that of massive spheroids (Cowie et al. 1996, Franceschini et al. 1999, De Lucia et al. 2006). All three discoveries imply that obtaining a complete census of accreting SMBH through the cosmic epochs and constraining accretion efficiency and feedbacks are crucial steps toward the understanding of Galaxy formation and evolution.

First attempts to constrain models for the formation and evolution of structure in the Universe using the evolving optical and X-ray AGN luminosity functions have been presented by Granato et al. (2001, 2004), Di Matteo et al. (2005), and Menci et al. (2004, 2005). In particular, the Menci et al. model links the evolution of the galaxies in the hierarchical clustering scenarios with the changing accretion rates of cold gas onto the central SMBH that powers the QSO (Cavaliere & Vittorini 2000). The results of this model were encouraging, in the sense that it predicts a trend of lower luminosity AGN to peak at increasingly lower redshift, as observed. However, from a quantitative point of view, the model overpredicts by a factor of about 2 the space density of low-to-intermediate luminosity (Seyfert like) AGNs at z=1.5-2.5 with respect to present X-ray observations. Furthermore, Marconi et. al. (2004, 2007 in preparation) derived a SMBH mass function from the X-ray selected AGN luminosity functions (e.g. La Franca et al. 2005) that falls short by a factor of about 2 to the "relic" SMBH mass function, evaluated using the $M_{BH} - \sigma_V$ / $M_{BH}-M_B$ relationships and the local bulge's luminosity function. The most likely explanation for both discrepancies is that present X-ray surveys, although very efficient to probe unobscured and moderately obscured AGN (with column densities up to a few 10^{23} cm^{-2}, the so-called Compton thin AGNs), miss most of the very highly obscured, but still strongly accreting objects, the so called Compton Thick AGNs, with a column density $N_H \gtrsim 10^{24}$ cm^{-2} (see Comastri 2004). Indeed, only a handful of the faintest sources in the Chandra deep fields may be Compton thick (see La Franca et al. 2005 and Tozzi et al. 2006). So we still may be viewing just the tip of the iceberg of the highly obscured AGN population. Compton thick objects may well be more common at high redshift, as suggested on theoretical ground by Silk & Rees (1998) and Fabian (1999) and on observational ground by e.g. Gilli et al. (2001), Worsley et al. (2004, 2006), and La Franca et al. (2005).

Compton thick AGN at $z \gtrsim 1$ can be recovered thanks to the reprocessing of the AGN UV emission in the infrared by selecting sources with AGN luminosities in the mid-infrared and faint near-infrared and optical emission (e.g. Martinez-Sansigre et al. 2005, 2006, Houck et al. 2005, Weedman et al. 2006a, 2006b). We investigate further this issue making use of the multiwavelength data

Electronic address: fiore@oa-roma.inaf.it
[1] INAF-OAR, via Frascati 33, Monteporzio, I00040, Italy
[2] Universita' di Roma La Sapienza, Italy
[3] ASI Science data Center, via Galileo Galilei, 00044 Frascati, Italy
[4] Max Planck Institut für extraterrestrische Physik, Giessenbachstrasse 1, D–85748 Garching bei München, Germany
[5] INAF-OABo, via Ranzani 1, Bologna, Italy
[6] Universita' di Bologna, via Ranzani 1, Bologna, Italy

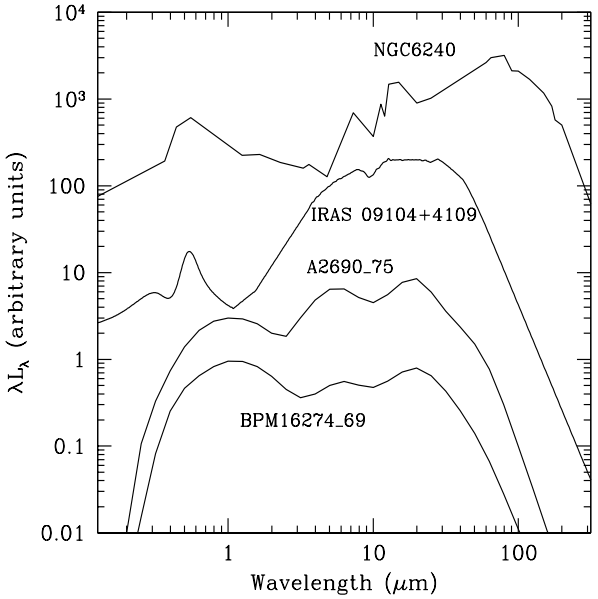

FIG. 1.— λL_λ spectral energy distributions of the four additional templates of sources hosting highly obscured AGNs used in this work. From top to bottom: NGC6240; IRAS09104+41091; HELLAS2XMM A2690_75 and BPM16274_69

obtained on the Chandra Deep Field South (Giacconi et al. 2002), one of the fields with the deepest coverage at optical, infrared and X-ray wavelengths.

A $H_0 = 70$ km s^{-1} Mpc^{-1}, Ω_M=0.3, $\Omega_\Lambda = 0.7$ cosmology is adopted throughout.

2. DATASETS AND SAMPLE SELECTION

The selection and spectroscopic identification of complete AGN samples from mid-IR surveys is a rather difficult task, because AGNs make only a small fraction of the full mid-IR source population. Using Spitzer IRAC colors results in samples significantly contaminated by star-forming galaxies (e.g. Lacy et al. 2004, Alonso-Herrero et al. 2006, Barmby et al. 2006, Polletta et al. 2006). Comparing the global observed Spectral Energy Distribution (SED) to AGN and galaxy templates proved to be more efficient in selecting AGN samples (Polletta et al. 2006, 2007). However, it is very difficult to assess the completeness of these samples given all complex selection effects. Furthermore, many obscured AGN may still be anyway missed by this technique.

We adopt in this paper a somewhat different approach. We do not pretend to select *all* AGN through optical and infrared photometry. As explained before X-rays are much more efficient in selecting unobscured (i.e. broad line AGNs) and moderately obscured AGNs. We concentrate our effort on highly obscured AGN only and we limit our analysis to the high infrared luminosity AGN population. The driving consideration is that differences between nuclear and star-formation emission are emphasized comparing the observed SEDs with galaxy templates over a range as broad as possible (also see Martinez-Sansigre et al. 2005,2006, Houck et al. 2005 and Weedman et al. 2006, Magliocchetti et al. 2007). Our primary objective here is to validate our obscured AGN selection criteria and assess the magnitude of the corresponding selection effects using a careful analysis of the deep X-ray data available on the CDFS.

2.1. *The GOODS-MUSIC catalog*

We use in this paper the latest version of the GOODS-MUSIC catalog (Grazian et al. 2006). We limit the analysis to the region fully covered by deep VLT/ISAAC near infrared photometry (143.2 arcmin^2) and to the sources with MIPS 24μm fluxes F(24μm)$>$ 40μJy (1729 sources). 24μm fluxes for all objects in the catalog, were obtained following the procedures described in De Santis et al. (2007).

The published version of the catalog contains z band and K band selected sources in the GOODS-south area. The revised version of the catalog used in this work includes 46 objects that are detected only in the 4.5μm band, i.e. their z and K magnitudes are below the chosen detection threshold. Only 4 of these sources do not have counterparts in the optical and/or in the near infrared images. At the flux limits adopted here, we do not detect any objects at 24μm that is not detected at shorter wavelengths. In the following we use for each entry of the catalog Vega magnitudes and cgs fluxes.

The GOODS-MUSIC catalog includes both monochromatic and total infrared luminosities, for the sources with a reliable spectroscopic or photometric redshifts. Total 8–1000μm luminosities were computed by integrating the best fit galaxy and AGN templates. Monochromatic luminosities were computed by interpolating the observed SEDs at the rest frame wavelength of interest. A large (factor of 10-30) systematic uncertainty is associated to the total infrared luminosity, being this dominated by the contributions at wavelengths of $\sim 100 - 1000\mu$m, well outside the infrared band used in this paper (1-24 μm). Different models can produce similar fits below 24μm but give rise to large differences in the total infrared luminosity. This systematic uncertainty is greatly reduced using the monochromatic luminosity at 5.8 μm (see e.g. Yan et al. 2007), since this wavelength is within the observed band up to z$\sim$3.2. For this reason in the following we make use of the infrared luminosity at 5.8μm (λL_λ(5.8μm)) to characterize the infrared power of the CDFS sources.

2.2. *Galaxy and AGN templates*

A detailed fitting of the observed SEDs using AGN and galaxy templates was also performed. Templates include passive galaxies, star-forming galaxies, unobscured AGNs and highly obscured AGNs. Spectral libraries include both empirical templates (Coleman et al. 1980 datasets, Polletta et al. 2007) and synthetic models (Bruzual & Charlot 2003, Fioc & Rocca-Volmerange 1997). We put particular care on the description of highly obscured AGNs. In addition to the templates presented by Polletta et al. (2007) we used four additional templates of sources hosting highly obscured AGNs (figure 1). The NGC6240 template includes U, B, V, J, H, K, IRAS and ISO photometry. The IRAS09104+41091 includes SDSS u, g, r, i, z photometry, B, V, R, J, H, K photometry, Spitzer IRAC and MIPS photometry, Spitzer IRS spectroscopy and IRAS photometry. For the two HELLAS2XMM sources we use the best fit SED model in Pozzi et al. (2007). These templates span a range of infrared to optical flux ratio significantly broader than the obscured AGN templates used by Polletta el al. (2007).

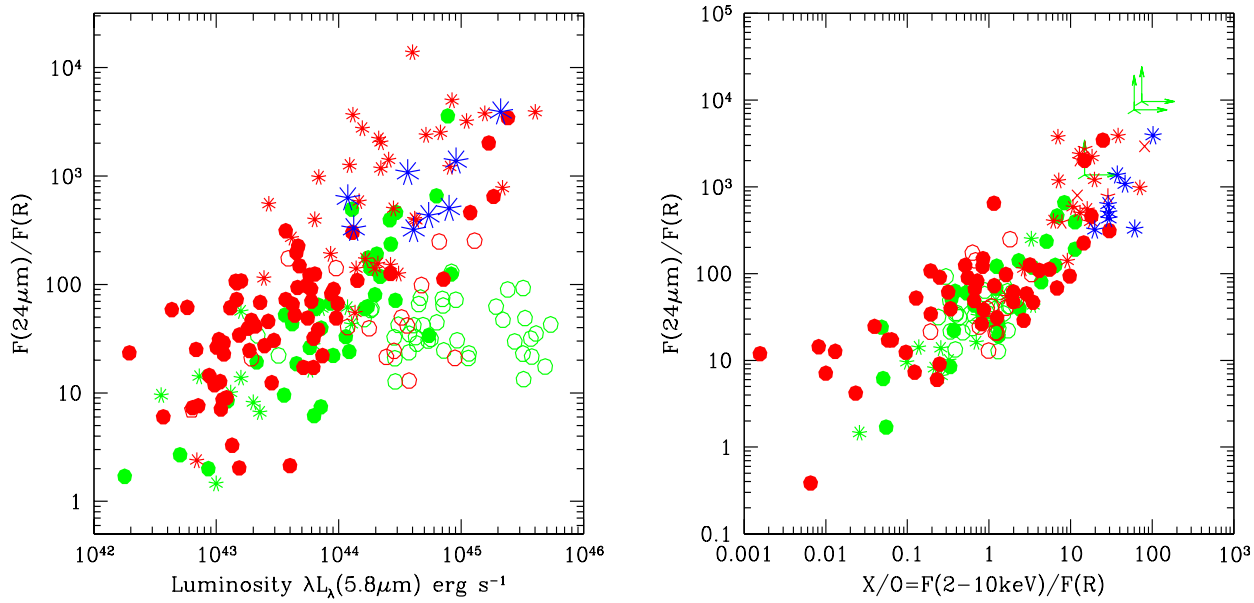

FIG. 2.— Left panel: F(24μm)/F(R) as a function of the 5.8μm luminosity for three X-ray source samples (GOODS-MUSIC, red symbols, ELAIS-S1, green symbols and HELLAS2XMM, large blue symbols , Pozzi et al. 2007). Open circles = type 1 AGN; filled circles = non type 1 AGN; stars = photometric redshifts. Note that F(24μm)/F(R) of non broad line AGN is strongly correlated with the luminosity at 5.8μm. Right panel: F(24μm)/F(R) as a function of the X-ray to optical flux ratio X/O for the same source samples. All symbols as in left panel; skeleton triangles = sources without optical counterpart.

2.3. *Photometric redshifts and SED fittings*

Photometric redshifts were derived by Grazian et al. (2006) fitting only the part of the SED dominated by the integrated stellar population, i.e. $\lambda < 5.5\mu$m (Grazian et al. 2006 and references therein). The synthetic models used are very accurate and complete in the treatment of the star-formation history and evolution of the stellar populations and of the dust content of the galaxy and its evolution. However, while dust extinction is easy to account for because it is a line of sight effect, dust emission and reprocessing is much more complicated to model, since it depends largely on the assumed geometry and covering fraction. Dust emission was therefore not considered in the models, and accordingly the bands above 5.5μm rest frame are ignored in these fits (see Grazian et al. 2006 for further details). This approach produces robust photometric redshifts ($\Delta z/(1+z) < 0.05$) for passive galaxies, star-forming galaxies and obscured AGNs, where the nuclear optical and infrared emission is completely blocked or strongly reduced by dust and gas along the line of sight. Unobscured AGNs with power law SEDs are excluded from this analysis (however, most of them have reliable spectroscopic redshift from Cimatti et al. 2002, Szokoly et al. 2004, Le Fevre et al. 2004, Vanzella et al.2005,2006, Mignoli et al. 2005).

To characterize each SED we repeated the fit to the observed SED with a library of empirical templates, fixing the redshift to the spectroscopic redshift or, if this is not present, to the photometric redshift obtained as described above. This library includes the 21 templates of passive galaxies, star-forming galaxies and AGNs by Polletta et al. (2007) and the four templates of systems hosting a highly obscured AGN in figure 1. The best fit template and normalization were used to measure monochromatic and total infrared luminosities.

2.4. *Optical, near infrared and mid infrared color selection*

The longest and shorthest wavelengths at which deep photometry is available on the Chandra Deep Fields are the 24μm mid-infrared band covered by Spitzer MIPS and the optical bands covered by HST ACS. 24μm sources with faint optical counterparts must be either luminous AGN whose optical nuclear emission is blocked by dust and gas, or powerful dusty-starburst galaxies. The Mid-infrared to optical flux ratio ([7]) can therefore be considered a rough estimator of obscured activity (both nuclear and star-formation) in galaxies.

Figure 2 shows F(24μm)/F(R) as a function of λL_λ(5.8μm), for three samples of X-ray sources. Unobscured AGNs (open symbols in figure 2) have F(24μm)/F(R) in the range 10-200, uncorrelated with λL_λ(5.8μm), as expected because the nuclear emission dominates both optical and mid infrared wavelengths. Conversely, obscured AGNs (filled symbols) have F(24μm)/F(R) spanning a broader range, and fairly correlated with λL_λ(5.8μm). This behavior resembles that of moderately obscured AGNs detected in X-rays, for which the X-ray to optical flux ratio (X/O) is strongly correlated with the X-ray luminosity (Fiore et al. 2003, Eckart et al. 2006). The nuclear optical-UV light of these objects is completely blocked, or strongly reduced by dust extinction, and the optical flux is dominated by the host galaxy. On the other hand, the 2-10 keV flux is reduced by only small factors, even for obscuring gas column densities of the order of a few$\times 10^{23}$ cm^{-2}. X/O is therefore a good estimator of the ratio between the nuclear flux and the host galaxy starlight

[7] F(24μm)/F(R); logF(R)=$-0.4 \times R - 22.5467$. R magnitudes have been obtained by interpolating the V and I magnitudes in the GOODS-MUSIC catalog provided by HST/ACS

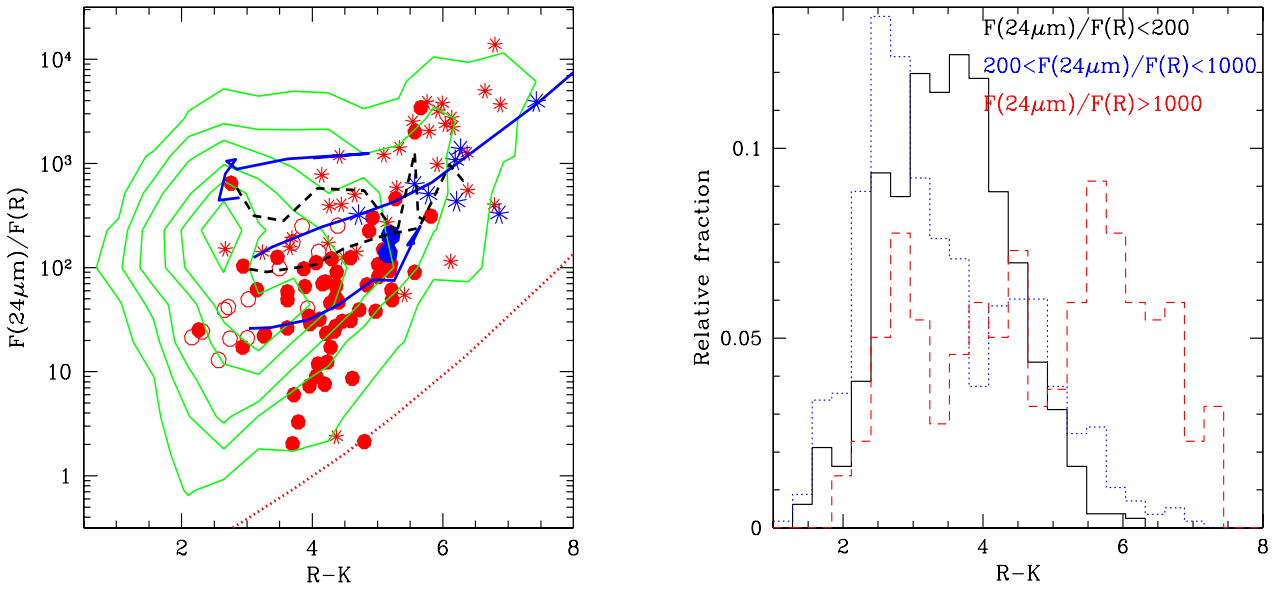

FIG. 3.— Left panel: F(24μm)/F(R) as a function of the R-K color for two X-ray source samples (GOODS-MUSIC and HELLAS2XMM, large symbols, from Pozzi et al. 2007). Open circles = type 1 AGN; filled circles = non type 1 AGN; stars = photometric redshifts. Isodensity contours of all GOODS-MUSIC 24μm sources are overlayed to the plot. The thick continuous lines mark the expectations of three obscured AGN SEDs with redshift increasing from 0 to 4 from left to right. The lower curve represents the colors of a typical low luminosity Seyfert 2 galaxy, the middle curve represents the colors of an obscured AGN from the Pozzi et al sample (A2690_75), the upper curve represents the colors of IRAS09104+41091. The black dashed lines are the expectations of the SEDs of two star-burst galaxies (M82, lower curve and Arp220, upper curve) for z=0-4. The dotted line is the expectation of a passive elliptical galaxy for z=0-4. Right panel: fraction of GOODS-MUSIC 24μm sources as a function of the R-K color in three F(24μm)/F(R) bins: solid histogram = F(24μm)/F(R)< 200; dotted histogram = 200 <F(24μm)/F(R)< 1000; dashed histogram = F(24μm)/F(R)> 1000.

flux. While the nuclear AGN X-ray luminosity can span several decades, the host galaxy R band luminosity has a moderate scatter, less than one decade, giving rise to the observed correlation between X/O and the X-ray luminosity. Perola et al. (2004), Mignoli et al. (2004), Brusa et al. (2005) and Cocchia et al. (2007) found that the high X/O sources tend also to be obscured in the X-rays, with column densities of the order of 10^{22-23} cm^{-2}. It is therefore possible to conclude that a high X/O ratio is a good indicator for both optical and moderate X-ray obscuration in high luminosity sources. Interestingly, the F(24μm)/F(R) of X-ray selected sources is strongly correlated with X/O (figure 2, right panel). This suggests that luminous Compton thick AGN, which are faint in X-rays because of the strong photoelectric absorption and Compton scattering, and cannot be selected using their X/O flux ratio, can be recovered using the F(24μm)/F(R) ratio.

Furthermore, since X-ray obscured AGNs tend to have red R-K colors (Brusa et al. 2005 and reference therein), one would also expect that Compton thick AGN have similarly red colors. Indeed figure 3 shows that the F(24μm)/F(R) of X-ray selected, obscured AGN is correlated with the R-K color, as expected. Figure 3 also shows the iso-density contours of all the GOODS-MUSIC 24μm sources with F(24μm)> 40μJy. Intriguingly, the iso-density contours become narrow in F(24μm)/F(R) at high R-K values and extend toward the region occupied by obscured X-ray selected AGN at high F(24μm)/F(R) and high R-K values. The bimodality at high values of F(24μm)/F(R) of the color distribution of the 24μm selected sources is evident in the rightmost panel of figure 3, which shows the fraction of GOODS-MUSIC 24μm sources as a function of the R-K color in three F(24μm)/F(R) bins. While at low and intermediate F(24μm)/F(R) values the distributions are peaked at R-K$\sim$ 2.5 − 3.5 and decrease smoothly toward higher R-K values, the distribution of the sources with F(24μm)/F(R)> 1000 shows a strong excess at R-K> 4.5.

It is interesting to note that most of the highly obscured AGN selected in the HELLAS2XMM survey on the basis of their high X-ray to optical flux ratio (Pozzi et al. 2007) have F(24μm)/F(R) higher than a few hundred, and all have R-K> 4.5. Their SEDs are characterized by a passive early-type galaxy in the optical and in the near infrared, and by an AGN component in the mid infrared. These SEDs redshifted up to z=4 are able to explain the extreme colors of the F(24μm)/F(R)> 1000 R-K> 4.5 sources, unlike the SED of even extreme star-forming galaxies like Arp220 (see figure 3 left panel). This strongly suggests that most of the F(24μm)/F(R)> 1000 R-K> 4.5 sources are powered by an active nucleus. Similar conclusions are found analyzing slightly different color diagrams, like F(24μm)/F(R) vs. F(24μm)/F(8μm) and F(24μm)/F(R) vs. F(3.6μm)/F(z).

3. X-RAY PROPERTIES OF EXTREME 24μM SELECTED SOURCES

Our candidate obscured AGNs are selected from the full 24μm GOODS-MUSIC sample with the request of having F(24μm)/F(R)> 1000 and R-K> 4.5. There are 135 such sources.

3.1. *Sources with a direct X-ray detection*

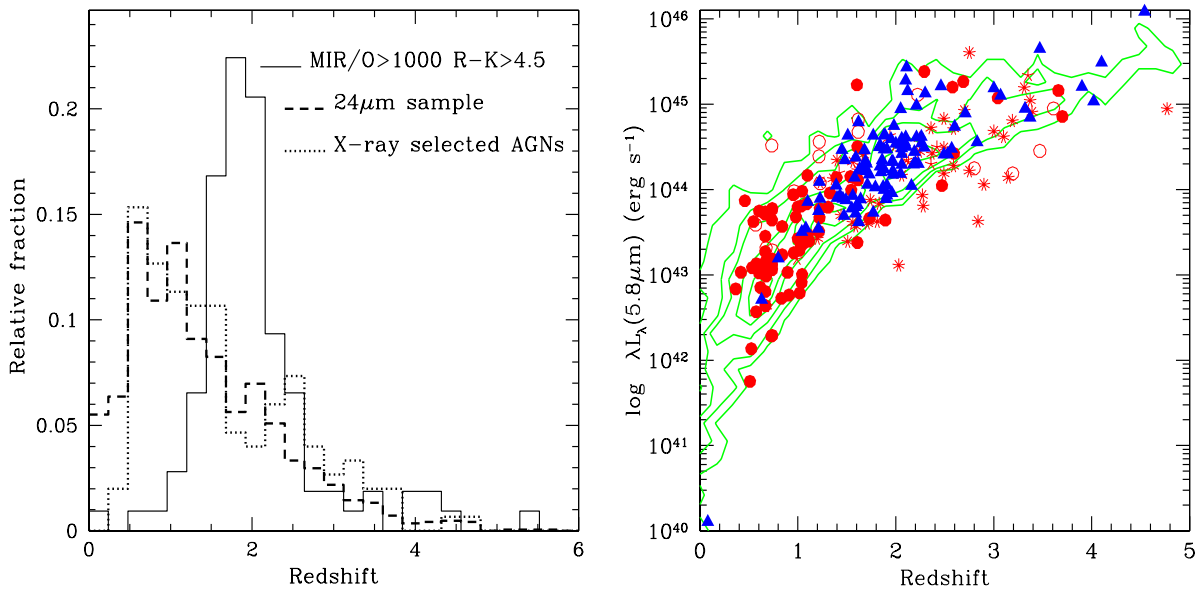

FIG. 4.— Left panel: the redshift distribution of the F(24μm)/F(R)> 1000 and R-K> 4.5 sources without direct X-ray detection (107 sources) compared to those of the full GOODS-MUSIC 24μm sample (1649 sources) and of the X-ray selected AGNs in the GOODS-MUSIC area (150 sources). Right panel: the redshift-infrared luminosity ($\log(\lambda L_\lambda(5.8\mu m))$) plane for the full 24$\mu$m GOODS-MUSIC source sample (isodensity contours); the CDFS X-ray AGN sample (open circles = type 1 AGN; filled circles = non type 1 AGN; stars = photometric redshifts); and the sample of F(24μm)/F(R)> 1000 and R-K> 4.5 sources without direct X-ray detection (filled triangles)

Eighteen of the 135 sources have an X-ray detection in Alexander et al. (2003). Four other sources are not formally detected but have more than 4-5 counts (after background subtraction) at the position of the 24μm source. In summary, 22 of the 135 sources (16%) have a significant X-ray emission directly visible in the Chandra images.

Three of these 22 sources have a spectroscopic redshift, with narrow line optical spectra, the other 19 have a photometric redshift in the GOODS-MUSIC catalog (see Section 2); the median redshift and its interquartile range of these 22 sources are 2.1 (0.5; hereinafter interquartile ranges are indicated in brackets after the median values).

The median monochromatic infrared luminosity at 5.8μm is 44.42 (0.37). The X-ray luminosities are in all cases higher than 10^{42} erg s^{-1}, making them bona-fide AGNs. The median logarithmic ratio between the 5.8μm and the 2-10 keV luminosities is 1.07 (0.32). As a comparison, the median of the same logarithmic ratio for the full GOODS-MUSIC X-ray sample (150 AGN with measured redshift) is 0.69 (0.47). The probability that the two distributions are drawn from the same parent population is $\lesssim$0.2%, using the Kolmogorov-Smirnov test.

The hardness ratios indicate in most cases a hard, possibly obscured, X-ray spectrum. Indeed, these sources are among the most obscured ones in the Tozzi et al (2006) analysis, all having column densities higher than a few$\times 10^{22}$ cm^{-2} and 2 having column densities as high as 10^{24} cm^{-2}.

Table 1 gives the breakdown of the best fitting templates (see Section 2) to the SEDs of these 22 sources. 15 SEDs are best fitted by one of the templates in figure 1.

3.2. *Sources without a direct X-ray detection*

TABLE 1
Table 1: template fits to the SEDs of the sources with F(24μm)/F(R)> 1000 and R-K> 4.5

Template	X-ray det.	Not X-ray det.
Ellipticals + S0	-	2
Spirals	-	1
M82+N6090+Arp220	-	35
I19254 + Mark231	4	17
Seyfert 1.8-2+red QSO	1	5
A2690_75 + BPM16274_69	5	34
IRAS09104+4109	9	11
N6240	1	1
Seyfert 1 +QSOs	2	1
Total	22	107

The total number of sources with F(24μm)/F(R)> 1000 and R-K> 4.5 and no direct X-ray detection is 111 (we excluded two sources which happen to lie within 5 arcsec from an X-ray source).

Four of these sources have a spectroscopic redshift, 99 have photometric redshift in the GOODS-MUSIC catalog. For four sources we could only compute a lower limit to the redshift. In conclusion, we have redshifts or limits for 107 sources. Both median redshift and infrared luminosity are similar to those of the 22 sources with a direct X-ray detection.

The redshift and infrared luminosities distributions of the F(24μm)/F(R)> 1000 and R-K> 4.5 sources are compared in figure 4 to those of the full GOODS-MUSIC 24μm and X-ray selected samples. The F(24μm)/F(R)> 1000 and R-K> 4.5 sources have a redshift distribution with median redshift 1.91 (0.30). Excluding the lower limits <z>=1.9 (0.28). This distribution is shifted toward higher redshifts than both the full GOODS-MUSIC 24μm source sample and the X-ray selected AGN sample (figure 4 left panel). The right panel of figure 4 shows that moderately obscured, X-ray selected sources

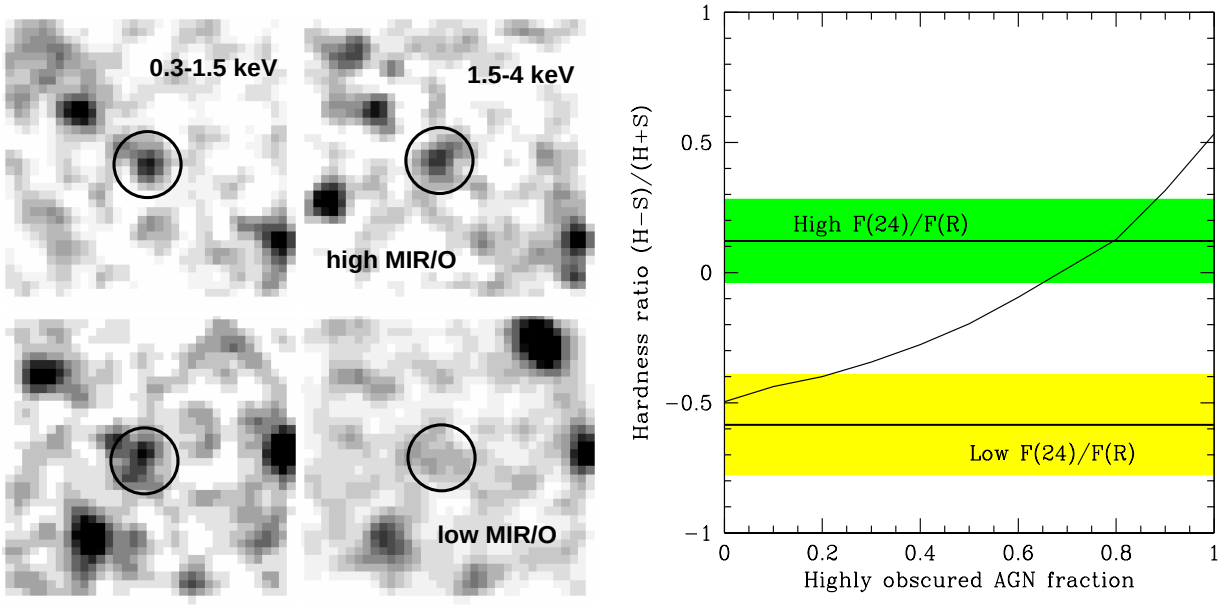

FIG. 5.— Left figure: stacked X-ray images of 24μm GOODS-MUSIC sources. Images have sides of 18 arcsec, central circles have 2 arcsec radii. Upper panels refer to 111 sources with F(24μm)/F(R)> 1000 and R-K>4.5; lower panels refer to 73 sources with F(24μm)/F(R)< 200 and R-K>4.5. Left panels are stacks in the S 0.3-1.5 keV band, right panels are stacks in the H 1.5-4 keV band. Right figure: the hardness ratio (H-S)/(H+S) of the counts in circles of 2 arcsec radii as a function of the fraction of highly obscured AGN for the sample of 111 24μm GOODS-MUSIC sources with F(24μm)/F(R)> 1000 and R-K>4.5. The solid curve is the result of Montecarlo simulations (see text for details); the two thick horizontal lines are the average hardness ratios measured for the F(24μm)/F(R)> 1000 and R-K>4.5 (upper line) and F(24μm)/F(R)< 200 and R-K>4.5 sources (lower line). The colored bands mark the hardness ratio statistical uncertainties.

are concentrated below z=1.5 and span a range of infrared luminosities $\log(\lambda L_\lambda(5.8\mu m)) \sim 42 - 45.3$ Their median 2-10 keV and infrared luminosities are 43.16 (0.56) and 43.84 (0.57) respectively. On the other hand, the F(24μm)/F(R)> 1000 and R-K> 4.5 sources are concentrated between z=1.2 and z=2.6 and have infrared luminosities from $\log(\lambda L_\lambda(5.8\mu m)) \sim 43.5$ to $\log(\lambda L_\lambda(5.8\mu m)) \sim 45.5$, with a median 44.34 (0.30), luminosities similar to that of the X-ray selected AGNs at the same redshift.

Table 1 gives the results of the template fits to the observed SEDs of the 107 sources with a redshift. In 65% of the cases AGN templates provide the best fit. The majority of these SEDs are best fitted by one of the templates in figure 1, the others are best fitted by one of the AGN templates of Polletta et al. (2007). Only one SED is best fitted by the template of a type 1 AGN. 36 SEDs are best fitted by star-forming galaxy templates (in 30 cases the best fit is obtained using powerful star-forming galaxy templates, like those of Arp220 and NGC6090). In conclusion, the results of the SED fitting analysis confirm that the majority of the sources with F(24μm)/F(R)> 1000 and R-K> 4.5 may be highly obscured AGNs. However, we remark that the results of the template fitting should not be always considered a quantitative determination of the nature of each single source, since in many cases different templates can produce fits with similar χ^2 in the observed optical to 24μm band, producing a degeneracy difficult to account for. Therefore, the results of the template fittings should only be taken as a qualitative indication of the population properties of the samples.

3.3. *X-ray stacking analysis*

To validate our highly obscured AGN selection sample and assess quantitatively the fraction of bona-fide AGNs in the F(24μm)/F(R)> 1000 and R-K> 4.5 sample, we performed a detailed "stacking" analysis of the X-ray data of the 24μm selected sources. Indeed, thanks to the low Chandra background, it is possible to increase the effective exposure time and derive average properties of undetected objects, using these stacking techniques: counts at the positions of known sources are co-added in order to probe X-ray emission substantially below the single source sensitivity limit.

We performed a stacking analysis of the 111 sources not directly detected in the Chandra 1 Msec X-ray image. As control samples we used the 22 sources with F(24μm)/F(R)> 1000 and R-K> 4.5 and an X-ray counterpart, a sample of sources with F(24μm)/F(R)> 1000 and R-K< 3.5 (51 sources after the exclusion of the sources directly detected in the X-ray image) and a sample of sources with F(24μm)/F(R)< 200 and R-K>4.5 (73 sources after the exclusion of the sources directly detected in the X-ray image). The total exposure times for the four source samples are 94 Msec, 19.5Msec, 43 Msec and 61 Msec respectively.

The top panels of figure 5a) show the X-ray stack of the 111 24μm sources with F(24μm)/F(R)> 1000 and R-K> 4.5 in two energy bands. This is compared to the stack of 73 sources with F(24μm)/F(R)< 200 and R-K> 4.5 and no direct X-ray detections (lower panels). We choose the bands 0.3-1.5 keV (soft band, S) and 1.5-4 keV (hard band, H) to keep the level of the internal background as low as possible and similar in the two bands. At a typical redshift of 2 these bands correspond to rest frame energies of 0.9-4.5 keV and 4.5-12 keV respectively. The stack of the high F(24μm)/F(R)

and high R-K sources produces a detection in both soft and hard bands, with count rates $(0.98 \pm 0.20) \times 10^{-6}$ counts/s and $(1.25 \pm 0.26) \times 10^{-6}$ counts/s in the two bands respectively (using a 2 arcsec radius extraction region). The hardness ratio H-S/H+S measured for this sample is therefore 0.12±0.15. Conversely, no detection in either bands is obtained for the stack of 51 sources with high F(24μm)/F(R) and low R-K, with 1σ upper limits of $\sim 2 \times 10^{-7}$ counts/s. The stack of the low F(24μm)/F(R) and high R-K sources produces a significant detection only in the soft band, with count rate $(1.89 \pm 0.32) \times 10^{-6}$ counts/s. The count rate measured in the hard band is significant at less than 3 σ and corresponds to $(4.9 \pm 1.9) \times 10^{-7}$ counts/s. The corresponding hardness ratio is H-S/H+S=-0.58±0.18. The stack of the 22 sources with F(24μm)/F(R)> 1000 and R-K> 4.5 and an X-ray counterpart produces a hardness ratio H-S/H+S= -0.06±0.01. In conclusion, the stack of the 111 sources with F(24μm)/F(R)> 1000 and R-K> 4.5 and without a direct X-ray detection produces a significant signal in both soft and hard X-ray bands. It is interesting to note that its hardness ratio suggests an average spectrum harder than even the average spectrum of the 22 sources with similar IR and optical colors but with a direct X-ray detection.

3.4. *Simulations to assess the fraction of obscured AGN in the 24μm source samples*

We used the observed flux in the stacked images, together with the hardness ratio H-S/H+S, to constrain the fraction of highly obscured AGN in the samples. To this purpose, we generated simulated X-ray count rates and hardness ratios as a function of the fraction of the AGN, assuming that the F(24μm)/F(R)> 1000 and R-K> 4.5 source sample is made by obscured AGNs and star-forming galaxies. We started from the observed redshift and infrared luminosities, and for the obscured AGN we assumed a log(λL_λ(5.8μm)/L(2-10 keV)) luminosity ratio chosen randomly in the range 0.4-1.2. The lower value is the typical ratio found by Silva et al. (2003) for low luminosity Seyfert 2 galaxies with column density log$N_H \lesssim 24$. It is also similar to the ratio found for the two HELLAS2XMM sources A2690_75 and BPM16274_69. The upper value is the ratio found for the powerful obscured QSO IRAS09104+4109 (Piconcelli et al. 2007).

For the star-forming galaxies we used a log(λL_λ(5.8μm)/L(2-10 keV)) luminosity ratio between 2 and 2.8. These two values are obtained assuming a total infrared to 2-10 keV logarithmic luminosity ratio of 3.6 (Ranalli et al. 2003) and correcting this for the ratio between the total infrared luminosity and the 5.8μm luminosity of powerful star-forming galaxies and spirals templates.

We further assumed that the star-forming galaxies are not obscured in X-rays, while the AGNs are highly obscured. For the latter objects, we adopted a flat logN_H distribution from 23 to 26 cm^{-2}.

For a given fraction of AGN in the sample, we first decide, using a random generator, whether each source is an AGN or a star-forming galaxy. Then, if the source turned out to be an AGN, we choose an absorbing column density using again a random generator and the assumed logN_H distribution. We computed unobscured 2-10 keV luminosities from infrared luminosities, and then X-ray fluxes by folding a power law spectrum with spectral energy index of 0.8 reduced at low energy by photoelectric absorption with a Chandra response matrix. For column densities $\gtrsim 10^{25}$ cm^{-2} we assumed that the direct emission is completely blocked by photoelectric absorption and Compton scattering. For these sources we assumed a reflection component with normalization 1/100 of the direct component and same spectral index.

A small fraction of the simulated count rates (20-30%) is higher than the Chandra detection limit. This was expected, given the fact that 22 out of 135 sources with F(24μm)/F(R)> 1000 and R-K> 4.5 do have X-ray counterparts. Since we are interested in the fraction of AGN in the sources not directly detected in the Chandra images, these count rates have been excluded from the following analysis.

The result of the simulations is shown in figure 5, right panel. According to our simulations, the average hardness ratio of the F(24μm)/F(R)> 1000 and R-K> 4.5 source sample without X-ray detection is reproduced if 80±15% of the sources in the sample are highly obscured AGNs. The hardness ratio of the sources with F(24μm)/F(R)< 200 and R-K> 4.5 is reproduced if the fraction of the obscured AGN is in the range 0-20%. Changing the assumptions made to produce the simulations within reasonable ranges changes only slightly this result.

The result of the simulations concerning the F(24μm)/F(R)> 1000 and R-K> 4.5 source sample is well consistent with the indication coming from the 1-24μm SED fitting with galaxy and AGN templates presented in the previous section.

4. DISCUSSION AND CONCLUSIONS

We selected a source sample with extreme mid-infrared to optical flux ratio (F(24μm)/F(R)>1000) and red optical colors (R-K>4.5) in the GOODS CDFS area. These sources are among the most luminous sources in the GOODS 24μm sample, because of the correlation of F(24μm)/F(R) with the infrared luminosity (see figures 2 and 4, right panel). The fraction of these sources not directly detected in the Chandra images produces a significant stacked signal in both Chandra soft and hard X-rays bands. A detailed analysis based on Montecarlo simulation shows that the stacked count rates and hardness ratios can be reproduced if this source population is dominated by highly obscured ($N_H >$ a few $\times 10^{23}$ cm^{-2}) AGNs.

This conclusion is further confirmed by the following consideration. If we assume that this source population is dominated by star-forming galaxies, we can use the observed infrared luminosity and the dust-corrected UV luminosities to derive two different estimates of star-formation rates. On one hand total infrared luminosities have been converted to a star-formation rate using the following formula: $SFR = L_{IR} ergs^{-1}/2.24 \times 10^{43} M_\odot/yr$, (Kennicutt 1998). On the other hand the UV star-formation rate is an output of the fits of the observed SEDs with synthetic models. These models have been obtained using the Bruzual & Charlot (2003) models, parametrizing the star-formation histories with a variety of exponentially declining laws (with timescales ranging from 0.1 to 15 Gyrs) and metallicities (from $Z =$

$0.02Z_\odot$ to $Z = 2.5Z_\odot$, see Grazian et al. 2006 and references therein for further detail). Dust extinction is added to all star-forming models, with $0 < E(B-V) < 1.1$ and a Calzetti attenuation curve. Given the very red colors of our objects in the optical bands, they are typically fit with star-forming templates with a large dust extinction ($E(B-V) > 0.5$), resulting in a star-formation rate much larger than what derived by a simple, dust free UV-to-SFR conversion.

The median logarithmic star-formation rate from infrared luminosity is 2.31 (0.59) $M_\odot$/yr. The median logarithmic UV star-formation rate is 0.83 (0.80)$M_\odot$/yr, a factor 30 lower. The large mismatch between these two estimates strongly suggests that the infrared luminosity of this source sample is not dominated by star-formation but rather by accretion. As a comparison, the median infrared and UV star-formation rates of the sources with F(24μm)/F(R)$<$ 200 and R-K$>$4.5 in our control sample are 1.26 (0.38) and 1.10 (0.30), consistent with each other, suggesting that the infrared luminosity of these sources is not dominated by nuclear accretion (in agreement with their X-ray hardness ratio, see previous section).

We can now compare the number of highly obscured AGNs selected at 24μm and not detected in X-rays, with the number of unobscured and moderately obscured AGNs directly seen in the X-ray images. To reduce the importance of complex selection effects we limit this analysis to the sources in the redshift bin 1.2-2.6. At z=2.6 the 5.8μm luminosity corresponding to the limit of 40μJy at 24μm is log(λL_λ(5.8μm))=44.3-44.2 for Seyfert 2,1.8 galaxy SEDs, and 44.4-44.5 for the four SEDs in figure 1. Assuming a log(λL_λ(5.8μm)/L(2-10 keV)) luminosity ratio in the range 0.4-1.2 implies unobscured 2-10 keV luminosities in the range 43.3-43.9. This suggests to limit the comparison to the sources with logL(2-10 keV)$>$ 43 and log(λL_λ(5.8μm))$\gtrsim$ 44.2.

In the 1.2-2.6 redshift bin there are at least 46$\pm$10 sources with F(24μm)/F(R)$>$1000, R-K$>$ 4.5, log(λL_λ(5.8μm))$\gtrsim$ 44.2 and no direct X-ray detection (80$\pm$15% of 57 sources), which are probably highly obscured AGNs, and 44 X-ray selected AGNs, 7 of which with broad lines in their optical spectra. The number of 24μm selected, presumably highly obscured AGNs, missed by the CDFS X-ray survey is therefore similar to the number of X-ray selected AGNs.

The median 5.8μm luminosity of the 57 F(24μm)/F(R)$>$1000 and R-K$>$ 4.5 sources without direct X-ray detection in the redshift and luminosity bins defined above is log(λL_λ(5.8μm))=44.48 (0.30), implying a median unobscured 2-10 keV luminosity in the range 43.3-44.1, adopting our assumption on the infrared to X-ray flux ratio. At z=2.6 these luminosities translate to X-ray fluxes between a few times 10^{-16} and 10^{-14} erg cm^{-2} s^{-1} , meaning that these sources would have been easily detected if they were not highly obscured.

We have compared our findings with the predictions of the La Franca et al. (2005) and Gilli et al. (2007) models. In the redshift bin 1.2–2.6 and in the area covered by our 24μm sample the La Franca et al. (2005) luminosity function predicts about 75 AGNs with logL(2-10 keV)$>$ 43, 20 of which with a column density $\gtrsim 10^{24}$ cm^{-2}. The absorption distribution adopted by the Gilli et al. (2007) AGN synthesis model for the Cosmic X-ray Background predicts about 40 Compton Thick AGNs with the same limits for redshift and luminosity. We find 46$\pm$10 24μm selected, highly obscured AGNs, a number about twice the La Franca et al. (2005) prediction but well consistent with the Gilli et al. (2007) prediction.

Marconi et. al. (2004, 2007 in preparation) derived a SMBH mass function from the X-ray selected AGN luminosity functions that falls short by a factor of about 2 to the "relic" SMBH mass function. This difference can be greatly alleviated adding the population of infrared selected, highly obscured AGNs to the AGN selected in the X-ray band below 10 keV.

Finally, we note that the population of infrared selected, highly obscured AGNs, can help in reconciling the predictions of models of galaxy evolution with the observed AGN number densities at z$\gtrsim 1-1.5$. Indeed, the Menci et al (2004) model predicts a number of low-to-intermediate luminosity AGNs at z=1.5-2.5 about twice with respect to that measured through X-ray 2-10 keV surveys (La Franca et al. 2005, Fiore 2006). We found above that in the redshift bin 1.2-2.6 the number of X-ray selected AGN with logL(2-10keV)$>$ 43 is comparable to that of the infrared selected, highly obscured AGNs. Therefore, adding together the two populations would give a total number density of AGNs similar to that predicted by the Menci et al. (2004) model. More detailed, quantitative, AGN number density calculations, spanning wider redshift and luminosity ranges, are beyond the purpose of this paper and will be presented elsewhere (Fiore et al. in preparation).

Most of the GOODS-MUSIC 24μm selected sources with high F(24μm)/F(R), high R-K and no X-ray detection have a very faint optical and near infrared counterpart, only 14% of the sample having R$\lesssim$26. Furthermore, only a handful of objects have a mid infrared flux high enough (F(24μm$\gtrsim$0.5mJy) to allow Spitzer IRS spectroscopy. The spectroscopic identification of $\sim$90% of the sample must therefore await the advent of ELTs or the launch of JWST.

Our analysis is limited to AGNs of intermediate luminosity at z$\sim$ 2. To extend the coverage of the luminosity-redshift plane requires a complementary observation strategy. Particularly useful to this purpose is the SWIRE survey, which has both Spitzer and optical medium-deep coverage on $\sim$ 50 deg^2 of sky. As an example, the SWIRE survey contains hundreds of sources with extreme F(24μm)/F(R) flux ratios and red optical-near infrared colors. Interestingly, several dozens of these extreme sources have 24μm flux higher than $\sim$ 1 mJy, allowing Spitzer IRS spectroscopy, and/or optical magnitude brighter than R$\sim$ 25, allowing spectroscopy with 8m class telescopes. Furthermore, all these sources are well within the reach of Herschel instruments between 75 and 500 μm. Such long wavelengths observations can greatly help in separating nuclear activity from star formation when the two components have comparable integrated luminosities, e.g. in low luminosity, Seyfert like, AGNs.

We are grateful to Fabio La Franca and Roberto Maiolino for useful discussions. We thank an anonymous referee for comments that helped improving the

presentation. After submission of this paper to ApJ we became aware of a work by a different group reaching similar conclusions (Daddi et al. 2007). We thank Emanuele Daddi for providing a copy of his manuscript before submission and for useful discussions. Part of this work was supported by ASI/INAF contracts I/023/05/0 and I/024/05/0 and by PRIN/MUR grant 2006-02-5203. Part of this work was supported by the Deutsches Zentrum für Luft– und Raumfahrt, DLR project numbers 50 OR 0207 and 50 OR 0405.

REFERENCES

Alexander, D. M., Bauer, F. E., Brandt, W. N. et al. 2003, AJ, 126, 539
Alonso-Herrero, A. et al. 2006, ApJ, 640, 167
Barmby, P., Alonso-Herrero, A., Donley, J.L. et al. 2006, ApJ, 642, 126
Bongiorno, A. et al. 2007, A&Asubmitted, astro-ph/0704.1660,
Brandt, W.N., Hasinger, G. 2005, ARA&A, 43, 1056
Brusa, M., Comastri, A., Daddi, E. et al. 2005 A&A, 432, 69
Bruzual, G., & Charlot, S. 2003, MNRAS, 344, 1000
Cavaliere, A. & Vittorini, V. 2000, ApJ, 543, 599
Cimatti, A. et al. 2002, A&A, 381, L68
Cocchia, F., Fiore, F., Vignali, C. et al. 2007, A&A, 466, 31
Coleman, G. D., Wu, C-C,& Weedman, D. W. 1980, ApJS, 43, 393
Comastri, A. 2004, in "Supermassive Black Holes in the Distant Universe", Ed. A. J. Barger, Kluwer Academic, vol. 308, p.245
Cowie L.L., Songaila, A., Hu, E.M., Cohen, J.G., 1996, AJ, 112, 839
Daddi, E. et al. 2007, ApJ submitted, astro-ph/0705.2832
De Lucia, G., Springel, V., White, S.D.M., Croton, D., Kauffmann, G., 2006, MNRAS, 366, 499
De Santis, C., Grazian, A., Fontana, A., Santini, P. 2007, New Astronomy, 12, 271
Di Matteo, T., Springel, V., Hernquist, L. 2005, Nature, 433, 604
Eckart, M.E., Stern, D., Helfand, D. et al. 2006, ApJS, 165, 19
Fabian, A.C. 1999 MNRAS, 308, L39
Ferrarese, L. & Merritt, D. 2000, ApJ, 539, L9
Fioc, M. & Rocca-Volmerange, B. 1997, A&A, 326, 950
Fiore, F., Brusa, M., Cocchia, F. et al. 2003, A&A, 409, 79
Fiore, F. 2006, in "AGN and galaxy evolution", Mem. SAIt, v.77, p.694, astro-ph/0603823
Franceschini, A., Hasinger, G., Miyaji, T., Malguori, D. 1999, MNRAS, 310, L5
Gebhardt, K., Kormendy, J., Ho, L. et al. 2000, ApJ, 543, L5
Giacconi, R., Zirm, A., Wang, J., et al. 2002, ApJS, 139, 369
Gilli R., Salvati, M., Hasinger G. 2001, A&A, 366, 407
Gilli R., Comastri A., Hasinger G. 2007, A&A, 463, 79
Granato, G.L., Silva, L., Monaco, P., Panuzzo, P., Salucci, P., De Zotti, G., & Danese, L. 2001, MNRAS, 324, 757
Granato, G.L., De Zotti, G., Silva, L., Bressan, A., Danese, L. 2004, ApJ, 600, 580
Grazian, A., Fontana, A., de Santis, C. et al. 2006, A&A, 449, 951
Hasinger, G. 2003, AIP Conf. Proc. 666, 227
Hasinger, G., Miyaji, T., Schmidt, M. 2005 A&A, 441, 417
Houck, J.R., et al. 2005, ApJ, 622, L105
Kennicutt, R.C., Jr. 1998, ARAA, 36, 189
Lacy, M. et al. 2004, ApJS, 154, 166
La Franca, F., Fiore, F., Comastri A. et al. 2005, ApJ, 635, 864
Le Fevre, O., Vettolani, G., Paltani, S., Tresse, L., Zamorani, G., Le Brun, V., Moreau, C., Bottini, D., Maccagni, D., Picat, J. P. et al. 2004, A&A, 428, 1043
Magliocchetti, M, Silva, L, Lapi, A. de Zotti, G., Granato, G.L., Fadda, D., Danese, L. 2007, MNRAS, 375, 1121
Marconi, A., Hunt, L. 2003, ApJ, 589, L21
Marconi, A., Risaliti, G., Gilli, R., Hunt, L. K., Maiolino, R., Salvati, M. 2004, MNRAS, 351, 169
Matt. G. 2000, A&A, 355, L31
Martinez-Sansigre, A., Rawlings, S., Lacy, M. et al. 2005, Nature, 436, 666
Martinez-Sansigre, A., Rawlings, S., Lacy, M. et al. 2006, MNRAS, 370, 1479
Menci N., Fiore, F., Perola, G.C, Cavaliere, A. 2004, ApJ, 606. 58
Menci, N., Fontana, A., Giallongo, E., Salimbeni, S. 2005 ApJ, 632, 49
Mignoli, M., Pozzetti, L., Comastri, A. et al. 2004, A&A, 418, 827
Mignoli, M., Cimatti, A., Zamorani, G., Pozzetti, L., Daddi, E., Renzini, A., Broadhurst, T., Cristiani, S., D'Odorico, S., Fontana, A. et al. 2005, A&A, 437, 883
Piconcelli, E., Fiore, F., Nicastro, F., Mathur, S., Brusa, M., Comastri, A., Puccetti, S. 2007, A&Ain press, astro-ph/0707.2465
Perola, G. C, Puccetti, S., Fiore, F. et al. 2004,A&A, 421, 491
Polletta, M., Wilkes, B., Siana, B. et al. 2006, ApJ, 642, 673
Polletta, M., Tajer, M., Maraschi, L. et al. 2007, ApJ, 663, 81
Pozzi, F., Vignali, C., Comastri, A. et al. 2007, A&A, 468, 603
Ranalli, P., Comastri, A., Setti, G. 2003, A&A, 399, 99
Silk, J., Rees, M.J. 1998, A&A311, L1
Soltan, A. 1982, MNRAS, 200, 115
Szokoly, G. P., Bergeron, J., Hasinger, G., Lehmann, I., Kewley, L., Mainieri, V., Nonino, M., Rosati, P., Giacconi, R., Gilli, R. et al. 2004, ApJS, 155, 271
Tozzi, P. , Gilli R. Mainieri V. et al. 2006, A&A, 451, 457
Ueda Y., Akiyama M., Ohta K., Miyaji T. 2003, ApJ, 598, 886
Vanzella, E., Cristiani, S., Dickinson, M., Kuntschner, H., Moustakas, L. A., Nonino, M., Rosati, P., Stern, D., Cesarsky, C., Ettori, S., et al. 2005, A&A, 434, 53
Vanzella, E., Cristiani, S., Dickinson, M., et al. 2006, A&A, 454, 423
Weedman, D.W., Le Floc'h, E., Higdon, S.J.U., Higdon, J.L., Houck, J.R. 2006a ApJ, 638, 613
Weedman, D.W., Soifer, B.T., Hao, L. et al. 2006b, ApJ, 651, 101
Worsley, M.A., Fabian, A. C., Barcons, X. et al. 2004, MNRAS, 352, L28
Worsley, M.A., Fabian, A. C., Bauer, F.E., Alexander, D.M., Brandt, W.N., Lehmer, B.D. 2006, MNRAS, 368, 1735
Yan, L., Sajina, A., Fadda, D., Choi, P., Armus, L., Helou G., Teplitz, H., Frayer, D., Surace, J. 2007, ApJ, 658, 778